

Contracting Arbitrary Tensor Networks: General Approximate Algorithm and Applications in Graphical Models and Quantum Circuit Simulations

Feng Pan,^{1,2,*} Pengfei Zhou,^{1,2,*} Sujie Li,^{1,2,*} and Pan Zhang^{1,3,4,†}

¹CAS Key Laboratory for Theoretical Physics, Institute of Theoretical Physics, Chinese Academy of Sciences, Beijing 100190, China

²School of Physical Sciences, University of Chinese Academy of Sciences, Beijing 100049, China

³School of Fundamental Physics and Mathematical Sciences,

Hangzhou Institute for Advanced Study, UCAS, Hangzhou 310024, China

⁴International Centre for Theoretical Physics Asia-Pacific, Beijing/Hangzhou, China

(Dated: June 30 2020)

We present a general method for approximately contracting tensor networks with an arbitrary connectivity. This enables us to release the computational power of tensor networks to wide use in inference and learning problems defined on general graphs. We show applications of our algorithm in graphical models, specifically on estimating free energy of spin glasses defined on various of graphs, where our method largely outperforms existing algorithms including the mean-field methods and the recently proposed neural-network-based methods. We further apply our method to the simulation of random quantum circuits, and demonstrate that, with a trade off of negligible truncation errors, our method is able to simulate large quantum circuits that are out of reach of the state-of-the-art simulation methods.

As a powerful method to alleviate the “curse of dimensionality” in high-dimensional modeling and data analysis, the tensor networks find wide applications in many areas of science and technology. In quantum many-body physics, tensor networks on lattices including the matrix product states (MPS) [1, 2], and the projected entangled pair states (PEPS) [3] have great success in the study of strongly correlated systems; in statistical mechanics, calculation of the partition function can be naturally converted to a tensor network contraction problem [4]; in computer science, the number of solutions of constraint satisfaction problems can be computed via tensor networks [5]; in data science, tensor networks and tensor decompositions are important tools for data compression and dimensionality reduction [6]. Recently, tensor network methods have been successfully extended to machine learning, in compressing a neural network [7], giving an efficient image classifier [8], and working as generative models in the unsupervised learning [9, 10].

Despite its wide use, however, the capability of the tensor networks is so far limited to either small-dimensional systems where the exact contraction is tractable, or high-dimensional systems only on regular lattices with local interactions, where there exist efficient contraction algorithms, e.g., the renormalization group [4, 11–13] and the block decimation [14]. On general systems with long range interactions and irregular connectivity (such as the graphs depicted in Fig. 1), the tensor network method is rarely applied, due to intractability of efficient contraction: to the best of our knowledge, there is no general method that exists for approximately contracting arbitrary tensor networks. This sets limitations on applying tensor networks to many areas, such as graphical models, statistical inference, and machine learning problems.

In this Letter we aim to break this limitation. We propose a general method for approximately contracting tensor networks on an arbitrary graph, based on a method we term as “MPS calculus”: the initial and intermediate tensors produced during the tensor contractions are represented, com-

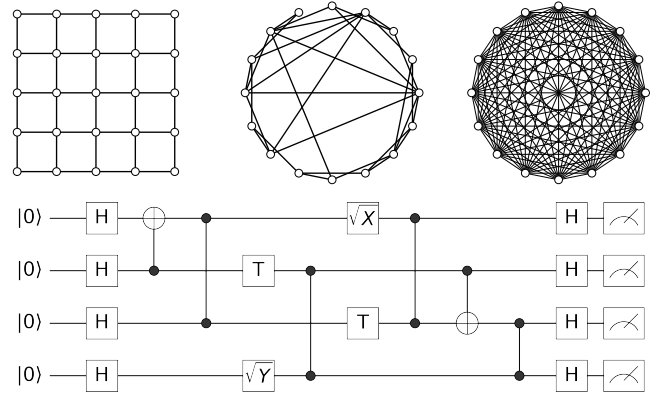


FIG. 1. Illustration of connectivity graph of the tensor networks we aim to contract: two-dimensional lattices, random graphs, fully connected graphs, and those defined by the quantum circuits.

pressed, and operated using the matrix product states in the canonical form. This allows us to deal with large intermediate tensors, which cannot be stored in the memory in its original form. During the contraction process we iteratively detect low-rank structures and apply low-rank approximations to reduce computational complexities of the contraction, using approaches analogous to the density matrix renormalization group (DMRG) [11], until the final result, a scalar Z , is obtained. We show applications of our method in graphical models, where Z represents the normalization factor of the joint distribution of a large number of random variables (i.e., the partition function in physics), and applications in quantum circuit simulations where Z represents a single amplitude of the quantum circuit.

Contracting arbitrary tensor network.— Our method relies on two ideas: (1) representing every tensor in the network by a matrix product state in the canonical form and (2) performing low-rank approximations based on the MPS representations during contraction. The matrix product state,

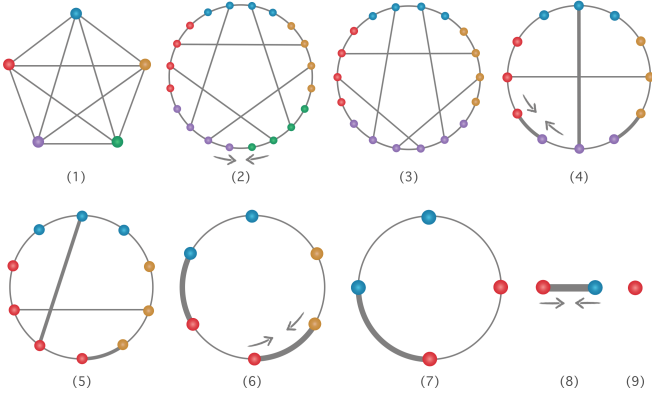


FIG. 2. Pictorial representation of our algorithm in contracting a tensor network with five tensors; see descriptions in main text.

also known as the tensor train in mathematics [15], is a one-dimensional tensor network composed of three-way tensors (and matrices in the boundary). A straightforward advantage of MPS is the parameter efficiency: an n -way tensor $\mathcal{A} \in \mathbb{C}^{d^n}$ can be represented by an MPS of virtual bond dimension χ with only $(n-2)d\chi^2 + 2d\chi$ parameters, using e.g., the DMRG [11]. With a large enough χ , the MPS can faithfully represent the original tensor and hence give an exact result. With limited computational resources, one would restrict the bond dimensions, performed as an approximation to the underlying raw tensor \mathcal{A} . Another characteristic of MPS is the canonical form, which can be achieved using QR decompositions or singular value decompositions [16, 17]. The first advantage of the canonical form is fixing the gauge degree of freedom, which eliminates the nonuniqueness in representing a raw tensor. More importantly, in the canonical form, the sum of discarded squared singular values corresponds to the loss of \mathcal{L}_2 norm of the whole MPS, rather than the local three-way tensor, which allows low-rank approximations on a global scope.

Given a tensor network composed of tensors $\mathcal{A}^{(1)} \dots \mathcal{A}^{(n)}$ and edges connecting the tensors, the high-level description of our algorithm, MPS calculus, is processed as follows: (1) Convert every tensor to a MPS. (2) If there are no edges left, return; else select an edge (ij) according to a contraction order. (3) "Contract" $\mathcal{A}^{(i)}$ and $\mathcal{A}^{(j)}$, store as $\mathcal{A}^{(i)}$; delete $\mathcal{A}^{(j)}$. (4) If $\mathcal{A}^{(i)}$ connects to $\mathcal{A}^{(k)}$ by two edges, "merge" the edges to a single edge using "swap" operations and low-rank approximations with singular value decomposition (SVD); then go to step 2.

A pictorial representation of the algorithm is sketched in Fig. 2 using a simple example of contracting a fully connected tensor network with five tensors, as shown in panel (1). In panel 2, every tensor that appears in 1 is converted to a MPS in the canonical form; During step 3-8, edges of the tensor network are contracted one by one, finally producing a scalar in step 9. For further details about the algorithm and order choices, please refer to the Supplemental Material and Refs [4, 11, 12, 16–25].

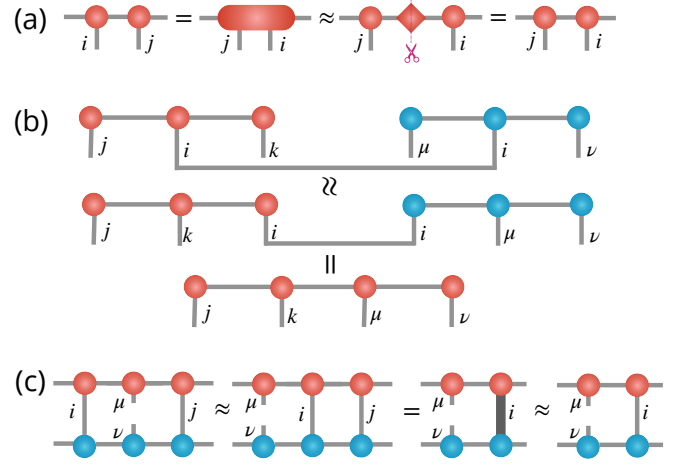


FIG. 3. Illustration of the (a) swap, (b) contract, and (c) merge operations. The scissor symbol indicates truncation of the singular values.

The contract operation is processed by merging two tensors to a single tensor by summing over the common index (say i) of them. Since all of them are MPSes, we need to move the common index i to the tail of the first tensor and to the head of the second tensor, using the swap operations. The swap operation switches the positions of two indices in the original tensor, by swapping two adjacent tensors in the mps, with a similar functionality as the swap gate in the quantum information. This operation increases entanglements of the MPS, and the maximum bond dimension could increase to $d\chi$, where χ denotes the virtual bond dimension of the MPS and d is the dimension of the physical indices. If $d\chi$ is greater than $\widehat{\chi}$, the preset limit on the virtual bond dimension, we canonicalize the MPS then truncate the bond dimension to $\widehat{\chi}$ during the singular value decomposition. An example of swap and contract are illustrated using tensor diagram notations in Fig. 7, where the scissor symbol indicates truncating of the dimension in the diagonal matrix.

After the contraction, the obtained tensor could have two indices, say j (with bond dimension d_j) and k (with bond dimension d_k) linked together to another tensor, due to existence of a triangle with three end tensors. In this case, we move indices j and k to adjacent positions using the swap operations and merge the two corresponding tensors to a three-way tensor with a larger physical bond dimension $d_j d_k$. If it exceeds \widehat{D} , the preset maximum physical bond dimension, we canonicalize both tensors, then do SVD together with a truncation on singular values to reduce the bond dimension from $d_j d_k$ to \widehat{D} . The process is illustrated in Fig. 7 (c).

The operations swap, contraction, and merge are repeated until the overall tensor network is finally contracted to a scalar Z . Our algorithm takes two parameters, the maximum physical bond dimension \widehat{D} and the maximum virtual bond dimension $\widehat{\chi}$ of the MPSes. The space complexity of the algorithm is bounded above by $O(\widehat{D}\widehat{\chi}^2)$, and the time complexity is dom-

inated by singular value decompositions adopted in the swap operations, which is $O(\widehat{D}^3\chi^3)$. Apparently, it is a polynomial algorithm that is able to contract arbitrary tensor networks with a limited amount of computational resources. Moreover, our method enjoys an efficient approximation scheme analogous to the DMRG method, which allows dynamically adjusting dimensions of the tensors. In the following text we will give applications of our algorithms, the inference and learning in the graphical models, and the simulation of quantum circuits, to empirically evaluate our method.

We noticed that in [26] the authors have proposed a general tensor network contraction algorithm by representing large intermediate tensors using the tree tensor network and reducing loop length using local singular value decompositions. Compared with [26], our method is capable of using larger bound dimension because the MPS has lower space complexity than the tree tensor network. Moreover, the canonical form of MPS allows more effective approximations.

Applications to graphical models— Graphical models are important tools for representing joint probability distributions over a large number of random variables that interact with each other, and find important applications in many fields in science and engineering. Without loss of generality, in this Letter we use the classic example of the graphical model, the Ising model and spin glasses in the statistical physics to demonstrate the power of our method. In this problem, the joint probability of n spins $\mathbf{s} \in \{\pm 1\}^n$ follows the Boltzmann distribution $P(\mathbf{s}) = \frac{1}{Z} \exp[-\beta E(\mathbf{s})]$, where $E(\mathbf{s})$ is the energy function of a configuration \mathbf{s} , β is the inverse temperature and Z is the partition function. Given a problem instance, an essential problem is computing the free energy $F = -\frac{1}{\beta} \ln Z$. However, this problem belongs to the class of $\#P$ problems hence it is hopeless to find polynomial algorithms for solving it exactly. In physics, many approximate algorithms have been developed. These include Markov chain Monte Carlo methods [27] and mean-field methods that parametrize a variational distribution by minimizing the variational free energy. Recently in [28], the mean-field methods have been extended by employing the autoregressive neural networks as a variational distribution, which, in principle has a strong expressive power.

Any probability distribution over discrete variables is a tensor, thus every graphical model can be converted to a tensor network by introducing copy tensors on each node of the graph, and matrices (or tensors) on each edge (or multi-body factor) of the (factor) graph. The computation of the partition function Z naturally translates to contraction of the tensor network defined exactly on the same graph. As an example, consider the celebrated pairwise Ising spin glass model with n variables: its energy function is defined as $E(\mathbf{s}) = -\sum_{(ij) \in \mathcal{E}} J_{ij} s_i s_j$, with \mathcal{E} denoting a set of edges and J_{ij} denoting couplings between two spins i and j . The parti-

tion function can be written formally as

$$Z = \sum_{\mathbf{s}} \prod_{(ij) \in \mathcal{E}} e^{\beta J_{ij} s_i s_j} = \text{Tr}(\mathcal{A}^{(1)} \times \mathcal{A}^{(2)} \times \cdots \times \mathcal{A}^{(n)}), \quad (1)$$

where the symbol \times represents contraction of tensors $\{\mathcal{A}^{(i)}\}$, each of which is given by contracting a copy tensor with matrices defined on the edges connected to node i ,

$$\mathcal{A}^{(i)} = \mathcal{I}_{d_i \times d_i} \times \mathbf{B}_{j \in \partial i} \times \mathbf{B}_{k \in \partial i} \times \cdots \times \mathbf{B}_{l \in \partial i}.$$

Here $\mathcal{I}_{d_i \times d_i}$ is a copy tensor, i.e. a diagonal tensor with order equal to the degree (number of neighbors) d_i of node i , with one on the diagonal entries and zero on the other entries. ∂i denotes the set of neighbors of node i , and the matrix $\mathbf{B}_{j \in \partial i}$ is a 2×2 matrix with $[\cosh(\beta J_{ij})/2]^{1/2} + [\sinh(\beta J_{ij})/2]^{1/2}$ on the diagonal and $[\cosh(\beta J_{ij})/2]^{1/2} - [\sinh(\beta J_{ij})/2]^{1/2}$ on the off-diagonal entries.

After converting the graphical model to tensor network, our method directly applies to computing free energy of the problem defined on arbitrary graphs. Observe that our algorithm is exact when the graph is a tree, because, by minimizing the size of the intermediate tensor, it performs variable eliminations iteratively on leaves of the tree and hence reduces to the belief propagation algorithm. On other graphs, our algorithm might generate truncation error ϵ_{SVD} . Empirically we observe that the error ϵ_{SVD} is several magnitudes smaller than the error of the obtained free energy ϵ_F , but so far it is not clear to us how to relate the two errors analytically. We subject to numerical experiments to demonstrate the performance of our algorithm.

The experiments are carried out using the Ising models and spin glasses on various of topologies, including 2D lattices, random graphs, small world graphs, and complete graphs. Our results on error of free energies are compared against mean-field methods including the naïve mean-field (NMF), Thouless-Anderson-Palmer equations (TAP), belief propagation (BP), and the neural-network-based variational autoregressive networks (VAN). On the 2D lattice without the external field, the graph is planar, so there are exact solutions [29]. Whereas on the other graphs, we adopt the exact (carefully designed) exponential algorithms [30] (in a reasonable time) to compute exact free energy values for the evaluations.

The results are shown in Fig. 4. We can see that, in all experiments, our method outperforms all mean-field methods and the neural-network-based methods, to a large margin. In regular random graphs, small world networks, and the Sherrington-Kirkpatrick model, our accuracy is only limited by the machine precisions (10^{-16}). In the experiments we choose $\widehat{D} = 50$ and $\chi = 500$, and the computational time on each instance is of a few seconds. Empirically, our method is faster than the mean-field methods and the neural-network-based methods. More results about the dependence of the bond dimensions and the computational time can be found in the Supplemental Material. Moreover, it is worth

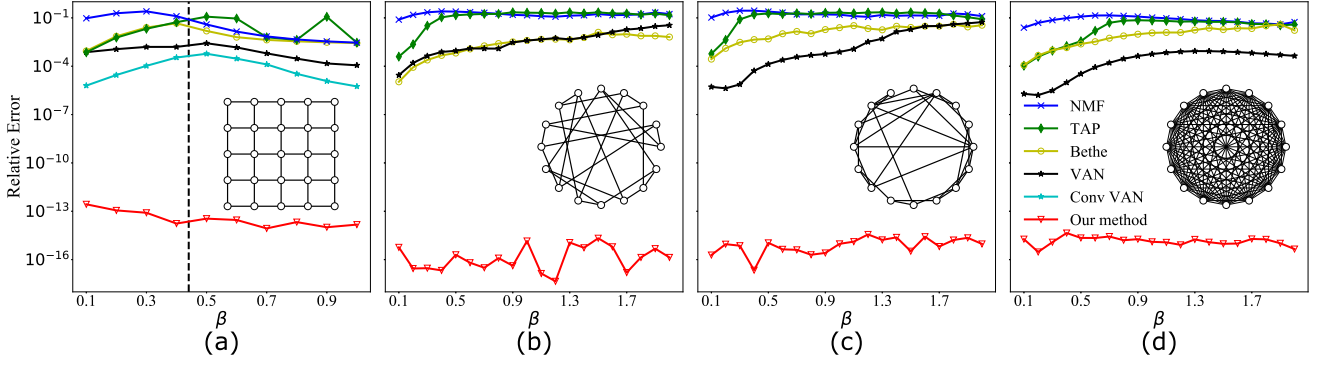


FIG. 4. Relative errors of the free energy to exact solutions obtained by different methods on various models. Insets: illustrations of the underlying connectivity graph with smaller sizes. (a) Ferromagnetic Ising model on a 16×16 square lattice; the exact solutions are given by [29], and the vertical dashed line represents the phase transition of an infinite system. (b) Ising spin glass model on random regular graphs of 80 nodes with degree $k = 3$; couplings J_{ij} are drawn from normal distribution with zero mean and unit variance. (c) Ising spin glass model on the Watts-Strogatz graphs of 70 nodes with average degree $c = 4$ and rewiring probability $p = 0.4$. The exact solutions are given by enumerating all configurations of feedback set of graphs [30]. (d) The Sherrington-Kirkpatrick model with $n = 20$ spins; exact solutions are given by enumerating 2^n configurations. Data points are averaged over 10 random instances.

noting that combining with the autodifferential for tensor networks [31] immediately gives our method an ability to perform learning tasks using graphical models. In the Supplemental Material, we give an example of using our method to learn a generative model [32–42] on hand-written digits of the MNIST dataset [43].

Application to quantum circuit simulations— The problem of computing free energy of graphical models is similar to the problem of computing single amplitude estimates of a superconducting quantum circuit [44], which can be treated as a graphical model with complex couplings. Classical simulation of quantum circuits is important for verifying and evaluating the computational advances of quantum computers [19, 21–23, 45, 46]. However, the near-term noisy intermediate-scale quantum circuits (including Google’s recently announced “supremacy circuit” [47]) are not perfect: each operation of them contains a small error. Thus, an important open question is whether approximate simulations of quantum circuits could beat the noisy quantum device. Answering this question apparently requires advanced studies of approximate algorithms for simulating quantum circuits.

Our method directly applies to approximate single-amplitude simulation of quantum circuits with any kind of connectivities, such as two-dimensional lattice [22, 23], and random regular graphs as considered in the quantum approximate optimization algorithm [48], after converting the initial state, the measurement qubit string, and the gates into tensors. The key difference between our method and existing methods for quantum circuit simulation is that, by detecting low-rank structures in the circuit, our method heavily reduces the computational complexity. Although this introduces SVD truncation errors, we will illustrate that at least in the shallow circuits the error is almost negligible. We perform experiments using standard random circuits on two-dimensional lattices [21–23], which iteratively apply single-qubit gates and

two-qubit controlled Z gates to the initial $|0, 0, \dots, 0\rangle$ state, and finally measure the amplitude of a specific qubit string. The generation protocol is described in detail in the Supplemental Material. We evaluate the performance of our method against the recently developed state-of-the-art exact tensor contraction method [23], which has a precisely predictable space and time complexity. With depth $d = 8$, our algorithm can handle circuits with at most $40 \times 40 = 1600$ qubits with SVD accumulated truncation error $\epsilon_{\text{SVD}} \leq 10^{-12}$ on a workstation with 64 GB memory in an hour. As compared in Fig. 5, the computational complexity of our method is much lower than the method of [23]. The right panel of Fig. 5 indicates that the method of [23] already costs at least 64 GB memory for storing the largest intermediate tensor with $L = 31$ and further requires 32 TB memory for handling $L = 40$. We note that so far our algorithm cannot handle the circuit with a large depth such as Google’s circuit [47] with a small SVD error, because the current implementation of our algorithm only works on a single workstation: this prevents us from using a large bond dimension.

Discussions— We have presented an algorithm for contracting arbitrary tensor networks, based on the matrix product state for automatic detecting of low-rank structures inside the tensor networks during the contraction process. We have demonstrated advances of our method in the inference and learning in graphical models and in simulation of shallow quantum circuits. The particular strength of our method is able to find the internal low-entanglement structures automatically in the irregular tensor networks. The MPS representation of tensors in our method naturally supports distributed storage. It is interesting to see how large a quantum circuit we can simulate if a supercomputer is accessible to our algorithm. Another interesting development is exploring learning with quantum circuits using our scheme and backpropagation. We hope more advanced arbitrary tensor network contraction

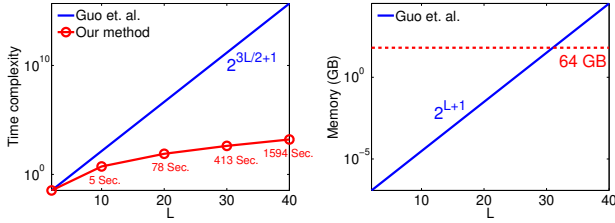


FIG. 5. Computational time and memory usage of our algorithm in simulating random quantum circuits with depth $d = 8$, comparing with the exact tensor network method of Guo et al. [23]. We ran our algorithm on a workstation with 64 GB memory (as indicated by the red dashed line). The blue lines with formulas in the figure represent the precise time and space complexity of the exact algorithm [23]. The memory usage is calculated based on double precision complex number. Each red point in the left panel is averaged over 10 random circuits, the error bars are much smaller than the symbol size.

methods inspired by our approach could fully release the numerical computational power of tensor networks to wider applications in science and engineering. A PYTHON implementation of our method is available at [49].

We thank Song Cheng, Haijun Liao, Chuang Wang, Lei Wang, Tao Xiang, Zhiyuan Xie, Haijun Zhou, and the BFS Tensor community for inspiring discussions, and Jinguo Liu for generating quantum circuits using *Yao.jl* [50]. P.Z. is supported by project QYZDB-SSW-SYS032 of Chinese Academy of Sciences, and the National Natural Science Foundation of China under Grants No. 11947302 and No. 11975294.

* These authors contributed equally.

† panzhang@itp.ac.cn

- [1] Guifré Vidal, “Efficient simulation of one-dimensional quantum many-body systems,” *Physical Review Letters* **93**, 040502 (2004).
- [2] Frank Verstraete, Juan J Garcia-Ripoll, and Juan Ignacio Cirac, “Matrix product density operators: simulation of finite-temperature and dissipative systems,” *Physical Review Letters* **93**, 207204 (2004).
- [3] Frank Verstraete and J Ignacio Cirac, “Renormalization algorithms for quantum-many body systems in two and higher dimensions,” *arXiv preprint cond-mat/0407066* (2004).
- [4] Michael Levin and Cody P Nave, “Tensor renormalization group approach to two-dimensional classical lattice models,” *Physical Review Letters* **99**, 120601 (2007).
- [5] Stefanos Kourtis, Claudio Chamon, Eduardo R Mucciolo, and Andrei E Ruckenstein, “Fast counting with tensor networks,” *arXiv preprint arXiv:1805.00475* (2018).
- [6] Andrzej Cichocki, Namgil Lee, Ivan Oseledets, Anh-Huy Phan, Qibin Zhao, Danilo P Mandic, *et al.*, “Tensor networks for dimensionality reduction and large-scale optimization: Part I low-rank tensor decompositions,” *Foundations and Trends® in Machine Learning* **9**, 249–429 (2016).
- [7] Ze-Feng Gao, Song Cheng, Rong-Qiang He, ZY Xie, Hui-Hai Zhao, Zhong-Yi Lu, and Tao Xiang, “Compressing deep neural networks by matrix product operators,” *arXiv preprint arXiv:1904.06194* (2019).
- [8] Edwin Stoudenmire and David J Schwab, “Supervised learning with tensor networks,” in *Advances in Neural Information Processing Systems* (2016) pp. 4799–4807.
- [9] Zhao-Yu Han, Jun Wang, Heng Fan, Lei Wang, and Pan Zhang, “Unsupervised generative modeling using matrix product states,” *Physical Review X* **8**, 031012 (2018).
- [10] Song Cheng, Lei Wang, Tao Xiang, and Pan Zhang, “Tree tensor networks for generative modeling,” *Phys. Rev. B* **99**, 155131 (2019).
- [11] Steven R White, “Density matrix formulation for quantum renormalization groups,” *Physical Review Letters* **69**, 2863 (1992).
- [12] Z. Y. Xie, J. Chen, M. P. Qin, J. W. Zhu, L. P. Yang, and T. Xiang, “Coarse-graining renormalization by higher-order singular value decomposition,” *Physical Review B* **86**, 045139 (2012).
- [13] Daiki Adachi, Tsuyoshi Okubo, and Syngye Todo, “Anisotropic tensor renormalization group,” *arXiv preprint arXiv:1906.02007* (2019).
- [14] R. Orús and G. Vidal, “Infinite time-evolving block decimation algorithm beyond unitary evolution,” *Physical Review B* **78**, 155117 (2008).
- [15] Ivan V Oseledets, “Tensor-train decomposition,” *SIAM Journal on Scientific Computing* **33**, 2295–2317 (2011).
- [16] Ulrich Schollwöck, “The density-matrix renormalization group in the age of matrix product states,” *Annals of Physics* **326**, 96–192 (2011).
- [17] Román Orús, “A practical introduction to tensor networks: Matrix product states and projected entangled pair states,” *Annals of Physics* **349**, 117–158 (2014).
- [18] Zhi-Yuan Xie, Hong-Chen Jiang, Qunjun N Chen, Zheng-Yu Weng, and Tao Xiang, “Second renormalization of tensor-network states,” *Physical Review Letters* **103**, 160601 (2009).
- [19] Igor L Markov and Yaoyun Shi, “Simulating quantum computation by contracting tensor networks,” *SIAM Journal on Computing* **38**, 963–981 (2008).
- [20] Eugene F Dumitrescu, Allison L Fisher, Timothy D Goodrich, Travis S Humble, Blair D Sullivan, and Andrew L Wright, “Benchmarking treewidth as a practical component of tensor network simulations,” *PloS one* **13**, e0207827 (2018).
- [21] Jianxin Chen, Fang Zhang, Mingcheng Chen, Cupjin Huang, Michael Newman, and Yaoyun Shi, “Classical simulation of intermediate-size quantum circuits,” *arXiv preprint arXiv:1805.01450* (2018).
- [22] Sergio Boixo, Sergei V Isakov, Vadim N Smelyanskiy, and Hartmut Neven, “Simulation of low-depth quantum circuits as complex undirected graphical models,” *arXiv preprint arXiv:1712.05384* (2017).
- [23] Chu Guo, Yong Liu, Min Xiong, Shichuan Xue, Xiang Fu, Anqi Huang, Xiaogang Qiang, Ping Xu, Junhua Liu, Shenggen Zheng, He-Liang Huang, Mingtang Deng, Dario Poletti, Wan-Su Bao, and Junjie Wu, “General-purpose quantum circuit simulator with projected entangled-pair states and the quantum supremacy frontier,” *Physical Review Letters* **123**, 190501 (2019).
- [24] Johnnie Gray and Stefanos Kourtis, “Hyper-optimized tensor network contraction,” *arXiv preprint arXiv:2002.01935* (2020).
- [25] Cupjin Huang, Fang Zhang, Michael Newman, Junjie Cai, Xun Gao, Zhengxiong Tian, Junyin Wu, Haihong Xu, Huanjun Yu, Bo Yuan, *et al.*, “Classical simulation of quantum supremacy circuits,” *arXiv preprint arXiv:2005.06787* (2020).
- [26] Adam Jermyn, “Automatic contraction of unstructured tensor networks,” *SciPost Physics* **8**, 005 (2020).

- [27] Fugao Wang and D. P. Landau, “Efficient, multiple-range random walk algorithm to calculate the density of states,” *Physical Review Letters* **86**, 2050–2053 (2001).
- [28] Dian Wu, Lei Wang, and Pan Zhang, “Solving statistical mechanics using variational autoregressive networks,” *Physical Review Letters* **122**, 080602 (2019).
- [29] Mark Kac and John C Ward, “A combinatorial solution of the two-dimensional ising model,” *Physical Review* **88**, 1332 (1952).
- [30] Feng Pan, Pengfei Zhou, Hai-Jun Zhou, and Pan Zhang, “Solving statistical mechanics on sparse graphs with feedback set variational autoregressive networks,” *arXiv preprint arXiv:1906.10935* (2019).
- [31] Hai-Jun Liao, Jin-Guo Liu, Lei Wang, and Tao Xiang, “Differentiable programming tensor networks,” *Physical Review X* **9**, 031041 (2019).
- [32] Yann LeCun, Yoshua Bengio, and Geoffrey Hinton, “Deep learning,” *Nature* **521**, 436–444 (2015).
- [33] Diederik P Kingma and Max Welling, “Auto-encoding variational bayes,” *arXiv preprint arXiv:1312.6114* (2013).
- [34] Laurent Dinh, David Krueger, and Yoshua Bengio, “Nice: Non-linear independent components estimation,” *arXiv preprint arXiv:1410.8516* (2014).
- [35] Laurent Dinh, Jascha Sohl-Dickstein, and Samy Bengio, “Density estimation using real nvp,” *arXiv preprint arXiv:1605.08803* (2016).
- [36] Danilo Rezende and Shakir Mohamed, “Variational inference with normalizing flows,” in *Proceedings of the 32nd International Conference on Machine Learning*, Proceedings of Machine Learning Research, Vol. 37, edited by Francis Bach and David Blei (Lille, France, 2015) pp. 1530–1538.
- [37] Benigno Uria, Marc-Alexandre Côté, Karol Gregor, Iain Murray, and Hugo Larochelle, “Neural autoregressive distribution estimation,” *Journal of Machine Learning Research* **17**, 1–37 (2016).
- [38] Aaron Van Oord, Nal Kalchbrenner, and Koray Kavukcuoglu, “Pixel recurrent neural networks,” in *Proceedings of The 33rd International Conference on Machine Learning*, Proceedings of Machine Learning Research, Vol. 48, edited by Maria Florina Balcan and Kilian Q. Weinberger (PMLR, New York, New York, USA, 2016) pp. 1747–1756.
- [39] Ian Goodfellow, Jean Pouget-Abadie, Mehdi Mirza, Bing Xu, David Warde-Farley, Sherjil Ozair, Aaron Courville, and Yoshua Bengio, “Generative adversarial nets,” in *Advances in neural information processing systems* (2014) pp. 2672–2680.
- [40] David H Ackley, Geoffrey E Hinton, and Terrence J Sejnowski, “A learning algorithm for boltzmann machines,” *Cognitive Science* **9**, 147–169 (1985).
- [41] Yann A LeCun, Léon Bottou, Genevieve B Orr, and Klaus-Robert Müller, “Efficient backprop,” in *Neural networks: Tricks of the trade* (Springer, 2012) pp. 9–48.
- [42] Diederik P Kingma and Jimmy Ba, “Adam: A method for stochastic optimization,” in *International Conference on Learning Representations* (2015).
- [43] Yann LeCun, Corinna Cortes, and Christopher J.C. Burges, “The mnist database of handwritten digits,” (1998), <http://yann.lecun.com/exdb/mnist> (Accessed on 19-November-2019).
- [44] Sergio Boixo, Sergei V Isakov, Vadim N Smelyanskiy, Ryan Babbush, Nan Ding, Zhang Jiang, Michael J Bremner, John M Martinis, and Hartmut Neven, “Characterizing quantum supremacy in near-term devices,” *Nature Physics* **14**, 595 (2018).
- [45] John Napp, Rolando L La Placa, Alexander M Dalzell, Fernando GSL Brandao, and Aram W Harrow, “Efficient classical simulation of random shallow 2d quantum circuits,” *arXiv preprint arXiv:2001.00021* (2019).
- [46] Roman Schutski, Danil Lykov, and Ivan Oseledets, “An adaptive algorithm for quantum circuit simulation,” *arXiv preprint arXiv:1911.12242* (2019).
- [47] Frank Arute, Kunal Arya, Ryan Babbush, Dave Bacon, Joseph C Bardin, Rami Barends, Rupak Biswas, Sergio Boixo, Fernando GSL Brandao, David A Buell, *et al.*, “Quantum supremacy using a programmable superconducting processor,” *Nature* **574**, 505–510 (2019).
- [48] Edward Farhi, Jeffrey Goldstone, and Sam Gutmann, “A quantum approximate optimization algorithm,” *arXiv preprint arXiv:1411.4028* (2014).
- [49] <https://github.com/panzhang83/catn>.
- [50] Xiu-Zhe Luo, Jin-Guo Liu, Pan Zhang, and Lei Wang, “Yao.jl: Extensible, efficient framework for quantum algorithm design,” *arXiv preprint arXiv:1912.10877* (2019).

Detailed description of the contraction process

The pseudo code of the algorithm is listed in the Algorithm 1. In the Algorithm list, the connectivity of the tensor network is denoted by a graph \mathcal{G} , its vertex set is denoted by \mathcal{V} , and its edge set is denoted by \mathcal{E} ; the notation D_{ij} represents the dimension of the bond (i, j) . We also give a simple example by contracting a tensor network composed of 5 nodes, each of which is a four-way tensor connecting to each other, with the step-by-step contraction process illustrated in Fig. 6.

Algorithm 1 MPS calculus

Input: Tensor networks with tensors $\mathcal{A}^{(1)} \dots \mathcal{A}^{(n)}$, and the connectivity graph $\mathcal{G}(\mathcal{V}, \mathcal{E})$; the maximum physical bond dimension \widehat{D} , the maximum virtual bond dimension $\widehat{\chi}$.

Output: Contraction result Z .

Convert every tensor to the MPS representation.

while $|\mathcal{V}| > 1$ **do**

 Select an edge (i, j) according to a contraction order.

 Move the local tensor corresponding to the edge (i, j) in the $\mathcal{A}^{(i)}$ to the tail position of the MPS representation.

 Move the local tensor corresponding to the edge (i, j) in the $\mathcal{A}^{(j)}$ to the head position of the MPS representation.

 Merge two MPSes $\mathcal{A}^{(i)}$ and $\mathcal{A}^{(j)}$ by contracting the edge (i, j) that connects them, resulting to new MPS $\mathcal{A}^{(i)}$; drop $\mathcal{A}^{(j)}$.

$\mathcal{E} \leftarrow \mathcal{E} \setminus \{(i, j)\}$

for $k \in \partial j$ **do**

$\mathcal{E} \leftarrow \mathcal{E} \setminus \{(j, k)\}$

if $k \in \partial i$ **then**

 Do *swap* operations to move the duplicated (i, k) edges to the adjacent positions in both MPSes $\mathcal{A}^{(i)}$ and $\mathcal{A}^{(k)}$.

 merge the adjacent local tensors, so that the two edges are combined, with a larger bond dimension $D_{k,i}$.

if $D_{k,i} > \widehat{D}$ **then**

 Canonicalize $\mathcal{A}^{(i)}$ and $\mathcal{A}^{(k)}$.

 Contract two tensors connected by the edge (i, k) .

 Do SVD on the unfolded matrix of the obtained tensor, and perform truncation on singular values to reduce $D_{k,i}$ to \widehat{D} .

end if

else

$\mathcal{E} \leftarrow \mathcal{E} \cup \{(i, k)\}$

end if

end for

$\mathcal{V} \leftarrow \mathcal{V} \setminus \{j\}$.

end while

Return $Z = \mathcal{A}^{(i)}$

Contracting two MPSes to a single MPS

As an example, consider merging two tensors $\mathcal{A} = \{a_{ijk}\}$ and $\mathcal{B} = \{b_{\mu\nu}\}$ into tensor $\mathcal{C} = \{c_{jk\mu\nu}\}$, where tensors are all in the MPS representation formulated as

$$a_{ijk} = \sum_{\alpha} \sum_{\beta} a_{j\alpha}^{(1)} a_{\alpha i \beta}^{(2)} a_{\beta k}^{(3)}, \quad (2)$$

$$b_{\mu\nu} = \sum_{\alpha} \sum_{\beta} b_{\mu\alpha}^{(1)} b_{\alpha i \beta}^{(2)} b_{\beta\nu}^{(3)}. \quad (3)$$

The process is illustrated using tensor diagram notations in Fig. 7. To ensure that summing over the index i results to another MPS, we first do *swap* on \mathcal{A} to switch the indices i and k

$$a_{ijk} = \sum_{\alpha} a_{j\alpha}^{(1)} a_{\alpha ik}^{(23)} \approx \sum_{\alpha, \beta} a_{j\alpha}^{(1)} \widehat{a}_{\alpha k \beta}^{(2)} \widehat{a}_{\beta i}^{(3)}, \quad (4)$$

where $\widehat{a}_{\alpha ik}^{(23)}$ are elements of the tensor created by contracting the index β ; and the last step of the above equation requires the singular value decomposition, which could introduce truncations in the singular values. Similarly, we apply the *swap* operation also on tensor \mathcal{B} , to switch indices of i and μ , giving

$$b_{\mu\nu} = \sum_{\beta} b_{\mu i \beta}^{(12)} b_{\beta\nu}^{(3)} \approx \sum_{\alpha, \beta} \widehat{b}_{i\alpha}^{(1)} \widehat{b}_{\alpha\mu\beta}^{(2)} b_{\beta\nu}^{(3)}. \quad (5)$$

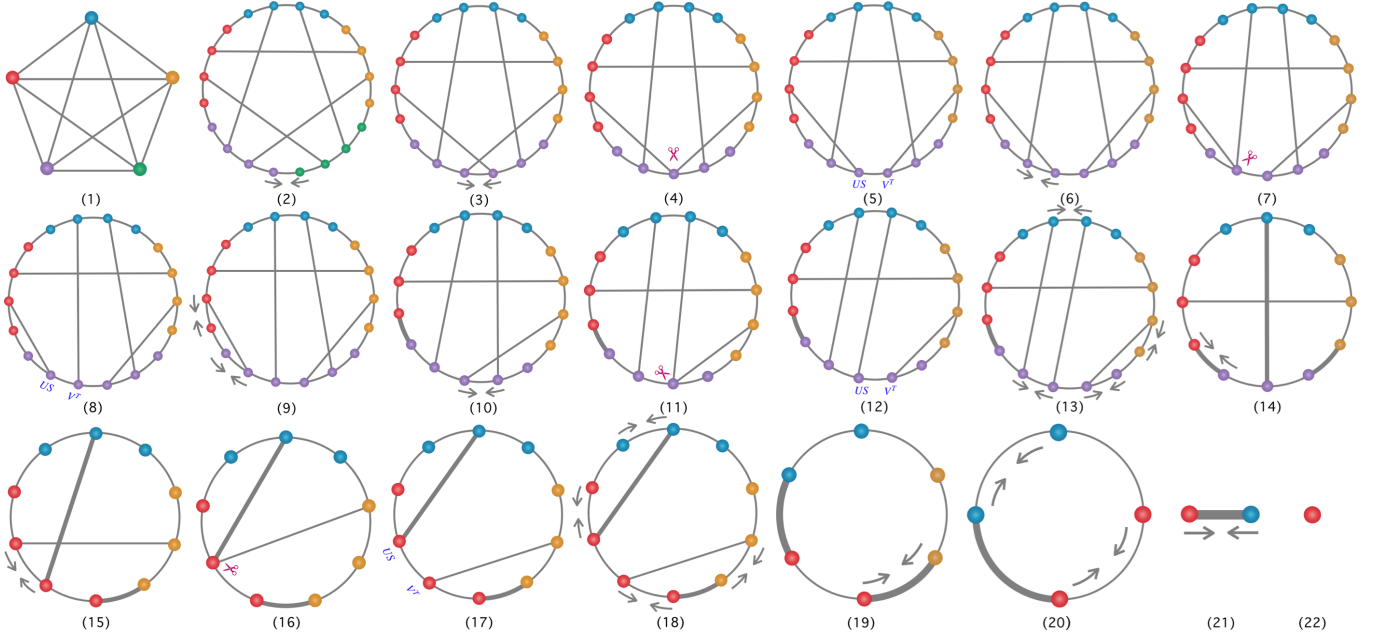


FIG. 6. Detailed process of contracting a tensor network with 5 nodes, each of which is a four-way tensor, as sketched in Fig. 2 of main text. The scissor symbols in the figures indicate applying SVDs on the matrices unfolded from the tensors. The tensors in the step (1) are the original four-way tensors connected to each other, forming a fully connected pentagon. The step (2) shows the MPS representation transformed from (1); the arrow indicates *contracting* two MPSes, that is, annihilating one color. As an example, the green MPS and the purple MPS is contracted to a longer purple MPS in (3). The steps (3) – (5) show the *swap* operation between two tensors in the purple MPS. To accomplish swapping, we contract two purple tensors first, then apply the SVD on the contracted tensor as shown in (3) and (4). Note that in (5), we keep the canonical form of the MPS. In steps (6) – (8), the *swap* operation is repeated until two tensors connecting the same pair of colors are switched to adjacent positions. In steps (9) and (10), we finish the *merge* step by contracting two tensors indicated by the arrow, producing a thick bond between red and purple MPSes. The steps (10) – (14) represent the *merge* between the purple-and-brown MPS pair and the purple-and-blue MPS pair. The steps (14) – (22) depict the procedure mentioned above repeatedly until a scalar left in the end of the whole contraction process.

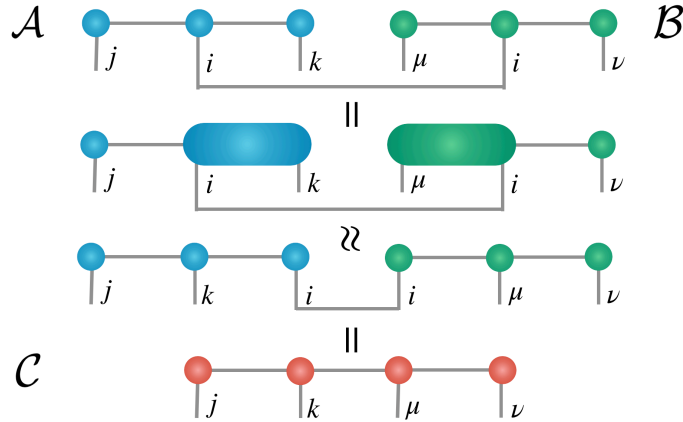


FIG. 7. Pictorial representation of the process of merging MPSes $\mathcal{A} = \{a_{jik}\}$ and $\mathcal{B} = \{b_{\mu i \nu}\}$ into another MPS $\mathcal{C} = \{c_{jk\mu\nu}\}$.

After performing the swap operations on both tensors, we can see that the index i locates at the tail position of the MPS representation of \mathcal{A} and at the head position of \mathcal{B} . Thus summing over index i results to a longer MPS \mathcal{C} , as shown in the bottom Fig. 7.

Canonical form of the MPS

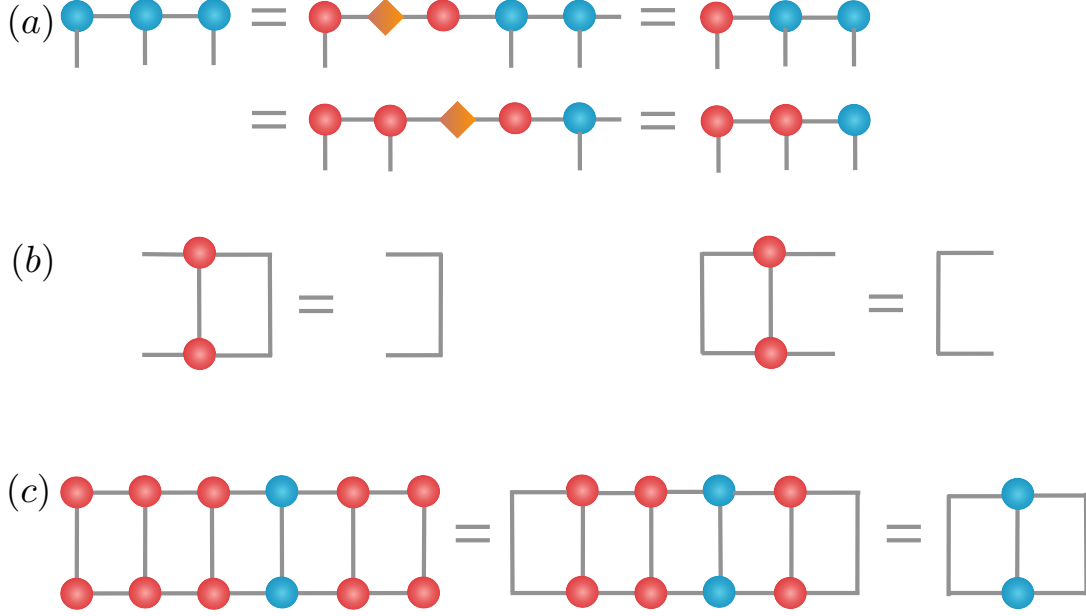


FIG. 8. Illustration of the canonical form. (a) process of left canonicalization. (b) property of isometries. (c) norm of the whole MPS converts to the norm of single 3-way tensor which is not an isometry. See descriptions in the text.

When a tensor in dimension 2^n is represented as an MPS composed of three-way tensors $\{\mathcal{A}^{(1)}, \mathcal{A}^{(2)}, \dots, \mathcal{A}^{(n)}\}$, every element of the tensor can be written as product of matrices

$$a_{i_1, i_2, \dots, i_n} = A_{i_1}^{(1)} \times A_{i_2}^{(2)} \times \dots \times A_{i_n}^{(n)}.$$

First notice that inserting identity matrices does not change anything, this suggests that there is a gauge degree of freedom which allows inserting any product of isometries U and U^\dagger into the above equation:

$$a_{i_1, i_2, \dots, i_n} = A_{i_1}^{(1)} \times U \times U^\dagger \times A_{i_2}^{(2)} \times \dots \times A_{i_n}^{(n)}.$$

This redundancy can be fully eliminated by the so-called canonical form [16, 17], which forces all 3-way tensors except one of them, say i -th tensor, to be isometry. If $i = n$ ($i = 1$), that is in the right (left) most position, the form is known as *left (right)* canonical position. Otherwise it is known as *mixed* canonical form.

An example of converting an MPS to the *left canonical* is illustrated in the top panel of Fig. 8. The blue tensors are not in isometry, while the red tensors are isometries, and the diamond represent diagonal matrix. The canonicalization is proceeded by

1. Performing singular value decompositions on the left-most tensor, produce $A^{(1)} = USV^\top$ where U and V are isometries, and S is a diagonal matrix storing singular values in the diagonal elements.
2. Absorbing S and V by the 3-way blue tensor in the middle, then perform singular value decompositions to the matrix unfolded by the tensor, producing isometries and diagonal tensors.
3. Keep the absorbing and SVD to every tensor in order, until all tensors, except the last one become isometry.

In addition to eliminating the gauge degrees of freedom, the second advantage of the MPS is that the (global) norm of the whole MPS becomes the norm of the local 3-way tensor which is the only one that is not an isometry. To show this more clearly,

consider performing partial trace over a 3-way isometry tensor \mathcal{A} , as illustrated in Fig. 8, it follows that

$$\sum_{\beta, \gamma} \mathcal{A}_{\alpha\beta\gamma} (\mathcal{A}^\dagger)_{\gamma\beta\alpha'} = \delta_{\alpha'}^\alpha.$$

With this good property, in a canonical form, when all tensors except a certain one are isometry, computing the norm of the MPS, as well as computing single-point and two-point measurements, can be translated to a computation of single-tensor quantity. An example is shown at the bottom panel of Fig. 8, where we can see that after the reduction the norm of the whole MPS becomes the norm of a single 3-way tensor. To our algorithm, this property is important for us to do precise approximations during the *merge* operation, where we need to do low-rank approximation between two connected MPSes by truncating the corresponding bond dimension, the canonical form transfers the local SVD truncations to a more global truncations involving the two MPSes, rather than involving only the two local tensors. We refer to [16, 17] for introductions of the matrix product states and the canonical form.

Contraction order

Much effort is devoted to obtain efficient contraction algorithms on these tensor networks mostly based on renormalization group (RG) method to keep topology as similar as the original regular lattices [4, 11, 12, 18]. However, when applied to problems out of physics such as graphical models, the underlying network connections being random, far from lattices, methods based RG seem to be in trouble. In essence, the key point is to find an optimal contraction order to contract all edges to get a scalar in which way computational memory and time is cost as little as possible. An important problem of the tensor network contraction is how to choose the edge order to eliminate one by one, which we refer to as *contraction order*. In [19], Markov and Shi showed that optimal contraction sequences correspond to optimal (minimum width) tree decompositions of a tensor networks line graph, relating the contraction sequence problem to a rich literature in structural graph theory. However finding the optimal tree decomposition for a general graph is a NP-hard problem, so usually one needs heuristic algorithms to find a good tree decomposition. Also notice that even equipped with the order given by the optimal tree decomposition, the algorithms for exact contraction in general is still an *exponential algorithm* with computational complexity grows exponentially with the tree width of the line graph. In [20] tree decompositions of line graph of the tensor network are performed for finding minimum tree width; recently in [24] authors adopted the community-detection based methods for cutting the whole task to small tasks corresponding to small communities, and in [25] the authors adopted the stem optimization which tries to find the major component that takes a majority of computational cost and optimize accordingly. Since we consider the approximate contraction using *polynomial algorithms*, in contrast with the exact contraction, the dimension of the intermediate tensors in our scheme are hard to predict, because whether there are low-rank structures that we can use to reduce the dimensionalities is not known a priori.

In this work, generally we adopt a greedy algorithm for sequentially selecting an edge from all remaining edges, which minimizes the dimension of the obtained tensor.

That is

$$(i, j) \leftarrow \underset{(\mu, \nu) \in \mathcal{E}}{\operatorname{argmin}} \left[\sum_{b \in \partial\mu} \log(D_{b,\mu}) + \sum_{b \in \partial\nu} \log(D_{b,\nu}) - 2 \log(D_{\mu,\nu}) \right].$$

For some specific problems we have other choices. For example for 2-D lattice we could simply take a Zig-Zag order which respect the 2D regular structure of the tensor network. Moreover, this can be improved using more sophisticated contraction ordering, for example using heuristic contraction orders given by tree decomposition of the line graph of the tensor network [19, 21–23], or given by partition-based methods [24, 25].

Dependences of the bond dimension \widehat{D} in the graphical model experiments

In our experiments on graphical models, \widehat{D} affects not only the running time but also the overall performance of the algorithm. In Fig. 9 we show how the results are influenced by changing the maximum physical bond dimension \widehat{D} . The experimental settings are identical to the main text. First, as expected, it is clearly shown that the relative error becomes smaller as \widehat{D} increasing for most situations. The only exception is with $\widehat{D} = 50$ on the 20-spin SK model, where the results have no difference compared to $\widehat{D} = 20$. This means $\widehat{D} = 20$ is large enough to deal with the 20-spin SK model at the β range considered here. In Fig. 10, time usage of our algorithm with different \widehat{D} are shown. Since a bigger \widehat{D} results to larger tensors, the time usage naturally increases. But for some cases, a bigger \widehat{D} occasionally changes the contraction order and avoid some approximation operations, leading to a lower running time than a smaller \widehat{D} .

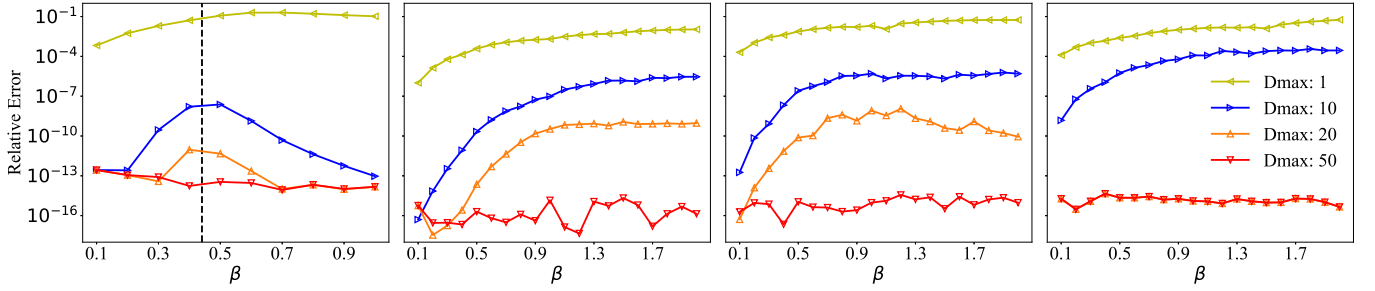


FIG. 9. Relative error of free energy on different models with varies \widehat{D} values, the experiment setting are identical to Fig. 3 of the main text.

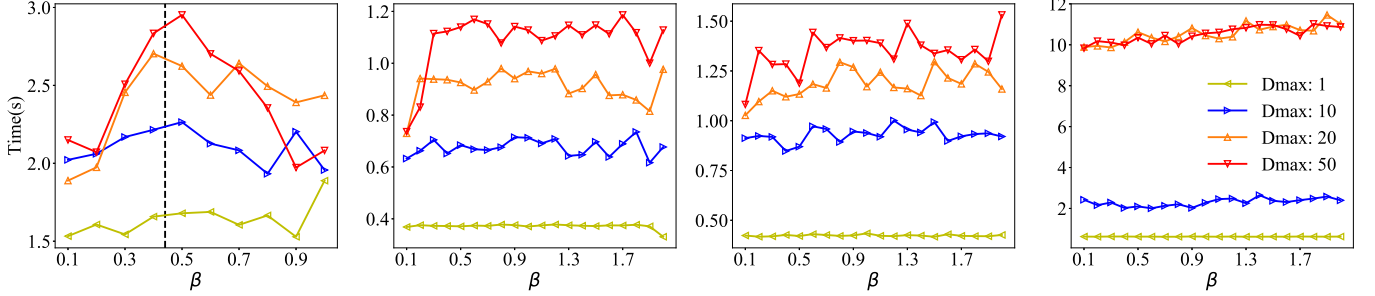


FIG. 10. Time consumptions of the tensor network contraction algorithm in the free energy experiment of main text.

Comparison between our method and the High Order Tensor Renormalization Group

In this section we compare with the High Order Tensor Renormalization Group (HOTRG) [12] method in terms of reproducing both free energy and correlation functions. The HOTRG is one of the representative tensor renormalization group method, and has been shown to outperform other TRG methods such as the Levin-Nave Tensor Renormalization Group [4] and the Anisotropic Tensor Renormalization Group [13]. The results are shown in Fig. 11. In the figure we have compared the relative error of free energy $\Delta F = -\frac{1}{\beta L^2} |\ln(Z) - \ln(Z^{\text{exact}})|$, and relative error of correlation functions $\Delta C = \sqrt{\sum_{(ij)} (C_{(ij)} - C_{(ij)}^{\text{exact}})^2}$, on the ferromagnetic Ising model on a $L \times L$ lattice with $L = 16$. The HOTRG stores many 4-way tensors with dimension \widehat{D}^4 during the contraction process, and our method stores many 3-way tensors with dimension $\widehat{D}\chi^2$. For a fair comparison, we force two methods to have the same space complexity, hence in our method we limit $\chi = \widehat{D}^{\frac{1}{2}}$. Moreover since comparisons are carried out only on 2-D lattices (because the HOTRG can not be applied to irregular lattices), rather than the general greedy contraction order, we choose to use a simple Zig-Zag contraction order, which selects tensors row by row.

From the figure we can see that with the same bond dimension \widehat{D} , our method works better than the HOTRG by giving smaller both free energy error and correlation error. In particular, with $\widehat{D} \geq 16$, in our method all error curves converge to almost machine precision, while the HOTRG requires $\widehat{D} \geq 36$ to reach a similar error.

Learning of graphical model using tensor networks

Generative learning in the unsupervised learning models the joint distribution of random variables in the given data and generates new samples from the learnt distribution. It is an important task in modern machine learning [32] and find wide applications in many areas of artificial intelligence. Fashion generative models include variational autoencoders (VAE) [33], normalizing flows [34–36], autoregressive models [37, 38] and generative adversarial networks (GANs) [39]. Here, we focus on a classical generative model known as the Boltzmann machine [40] with no hidden variables, which is also known as the inverse Ising model which is the maximum entropy model given the pairwise measurement of data. Using this example we demonstrate that our method for contracting the Ising model can be directly used for learning tasks. The objective function of the learning

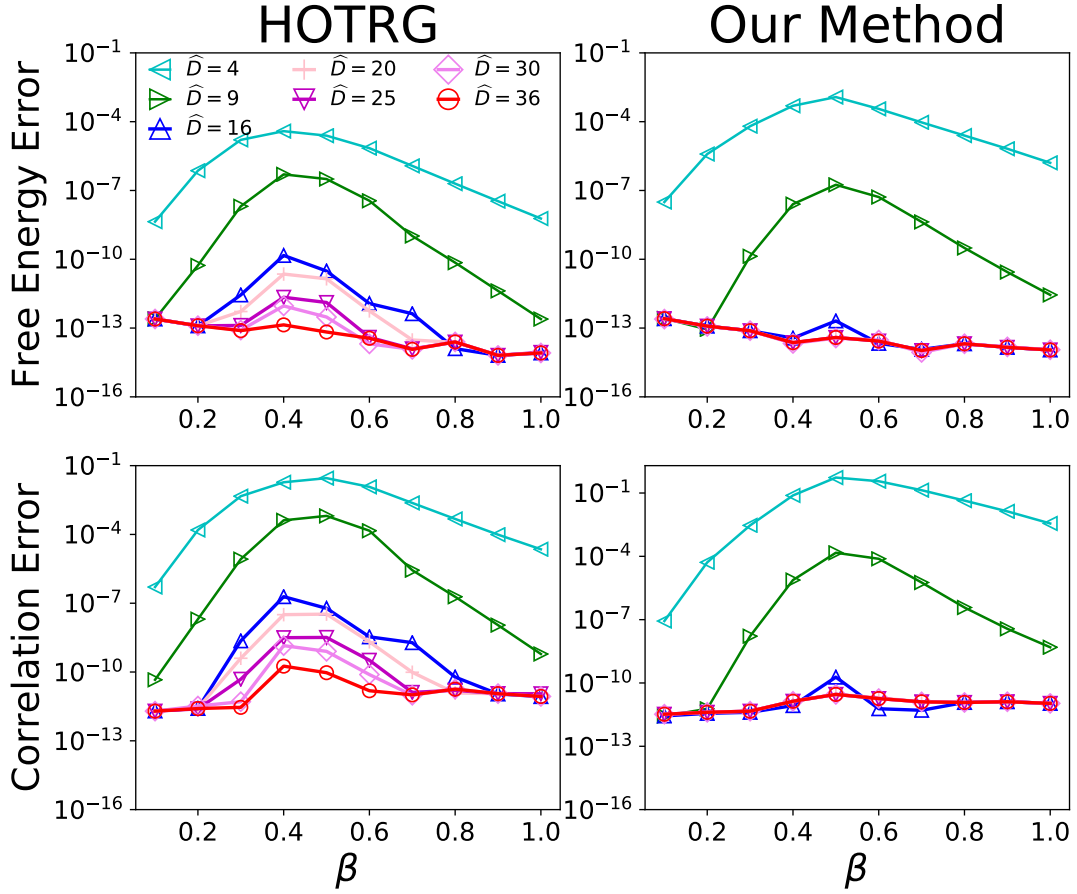


FIG. 11. Relative error of free energy (*Top*) and correlations (*Bottom*) to exact solutions, of the High Order Tensor Renormalization Group (HOTRG) [12] and our method, on the ferromagnetic Ising model on 16×16 square lattice with different inverse temperature β . Both HOTRG and our method have the same maximum physical bound dimension $\hat{D} = 4, 9, 16, 20, 25, 30, 36$ from top to bottom.

using an Ising model is the the negative log-likelihood \mathcal{L} , which we aim to minimize:

$$\begin{aligned} \mathcal{L} &= -\frac{\log P(\mathbf{X})}{N} = -\frac{\log \prod_i P(\mathbf{x}_i)}{N} \\ &= -\frac{\beta}{N} \sum_i \left(\sum_{(mn) \in \mathcal{E}} J_{mn} x_{i,m} x_{i,n} + \sum_m h_m x_{i,m} \right) + \log Z \end{aligned} \quad (6)$$

In the last equation, \mathbf{X} is the dataset, \mathbf{x}_i is the i -th data, N is the size of dataset and \mathcal{E} represents edges of graphical model we employ. In classical machine learning method, the partition function $\log Z$ appearing in the log-likelihood is difficult to compute, and people usually use approximated method such as the *contrastive divergence*. Fortunately our method provides a relatively fast and accurate way to calculate $\log z$. Essentially, by setting the derivative of \mathcal{L} with parameters J_{mn} (couplings) and h_m (external fields) to be zero, we can get

$$\begin{aligned} \beta C_{data} &= \frac{\beta}{N} \sum_i x_{i,m} x_{i,n} = \beta C_{model} = \frac{\partial \log Z}{\partial J_{mn}} \\ \beta M_{data} &= \frac{\beta}{N} \sum_i x_{i,m} = \beta M_{model} = \frac{\partial \log Z}{\partial h_m}. \end{aligned} \quad (7)$$

The model parameters $\{J_{mn}\}$ and $\{h_m\}$ can be learnt by matching the moments of the model with the moments of data. We emphasis that, here we do not even need to calculate the correlations and magnetizations, because the gradient on J_{mn} and h_m can be estimated directly by taking derivative of the loss function by using the back-propagation algorithm. Then the learning

can be carried out by utilizing a modern deep learning optimizer such as the stochastic gradient descent (SGD) [41] and the ADAM [42] to update the parameters.

As a demonstration, we perform experiments on the handwritten digits of the MNIST dataset [43] to show how to learn an Ising model from data using our TN method combined with the back-propagation algorithm. For preparation, we reshape 28×28 binarized images to 14×14 for faster contractions. Our graphical model is based on 2D square lattice with additional diagonal connections and second nearest neighbors connections. As an demonstration, we use only first five images of MNIST as training set for learning the model.

After training through stochastic gradient descent, the Ising model displays the similar distribution as the empirical distribution of the training data, and we can generate images by sampling from the distribution that our model has learned. Here we adopt traditional Markov Chain Monte Carlo (MCMC) to sample from the model, the samples are shown in Fig. 12. We can see that the images are well presented and similar to the training images. The negative loglikelihood obtained is 2.41 which is very close to the lower bound $\ln 5 = 1.61$.

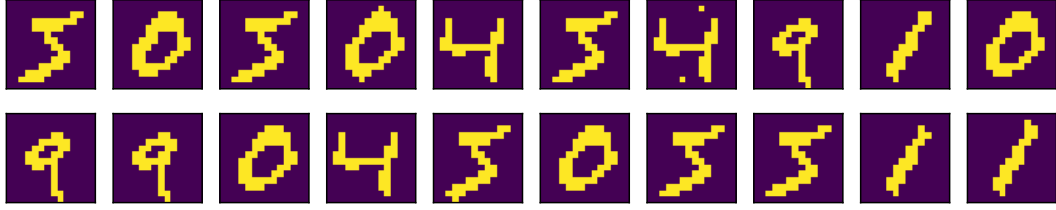


FIG. 12. MCMC samples of Ising model learnt from 5 handwritten images of the MNIST dataset.

Protocol for generating random quantum circuits

The random quantum circuits with depth d used in our experiments are generated as follows:

1. Apply a Hadamard gate to each qubit.
2. Apply controlled-Z gates organized in one of the eight layouts as shown in Fig. 13 once a time alternatively, then apply a randomly chosen gate from $\{T, X^{1/2}, Y^{1/2}\}$ to each qubit which is not acted by the CZ gates.
3. Repeat steps 2 for $d - 1$ times.
4. Apply a Hadamard gate to each qubit.

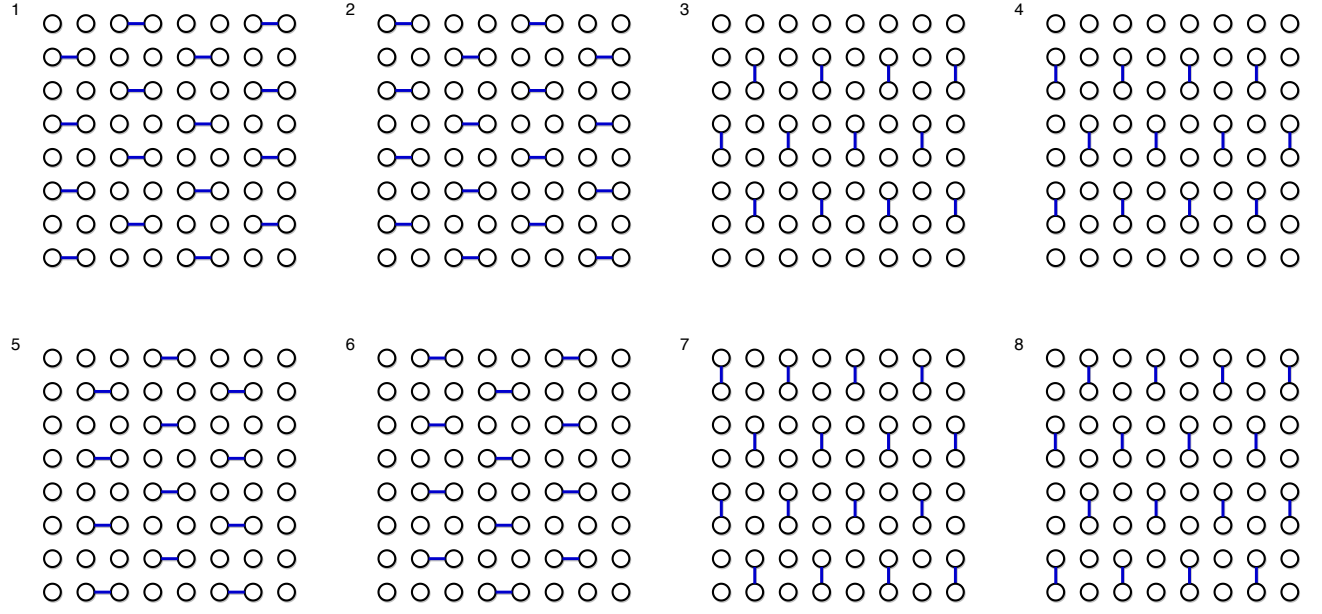


FIG. 13. Choices of the two-qubit-gate layers in generating random quantum circuits.